Int. J. Multiphase Flow Vol. 19, No. 6, pp. 921–941 1993
Printed in Great Britain.

0301-9322/93 $6.00 + 0.00

EXPERIMENTAL DETERMINATION OF GAS MIGRATION VELOCITIES WITH NON-NEWTONIAN FLUIDS

A. B. JOHNSON and D. B. WHITE†
Department of Fluid Mechanics, Schlumberger Cambridge Research, P.O. Box 153, Cambridge CB3 0HG, England

(Received 15 November 1991; in revised form 8 September 1993)

Abstract—The two-phase flow characteristics of gas in non-Newtonian fluids are important in many applications in various industries. Typical examples include the food processing industry, where it is sometimes desirable to aerate melted chocolate; also the chemical industry, where it is desirable to de-aerate non-drip paint. In the field of oil exploration the drilling mud is non-Newtonian. It is used for cooling the drilling bit, removing the drilled cuttings and maintaining the bottom hole pressure. Typical drilling muds have a yield stress to prevent sedimentation of drilled cuttings; they are also shear thinning to reduce pumping power and circulating pressures. An influx of gas into the wellbore is known as a gas kick and can lead to a blowout. One of the critical parameters in the evolution of a kick is the rate at which the gas influx rises up the well through the non-Netwonian drilling mud. The main parameters governing the gas velocity are the wellbore geometry (typically large annulus), the well inclination (vertical to horizontal), the volumetric flow rates, the volumetric gas fraction (0–100%) and the fluid rheology (yield stress and shear thinning).

An experimental programme was set up at Schlumberger Cambridge Research to examine two-phase flows in large pipe and annular geometries using non-Newtonian liquids. The experiments were carried out in a 15 m inclinable flow loop, where air injection was used for the gas phase and aqueous xanthum gum solutions as well as water were used for the liquid. Using an instrumented test section it was possible to measure mean and spatially resolved void fractions together with gas and liquid velocities over a range of two-phase flow conditions. The results for vertical conditions showed that the air–water flows could be characterized as bubbly flows up to a void fraction of 15%, slug flow over 30% and transitional between. For the viscous muds the transition to slug flow occurred below a void fraction of 7.5%. This meant that for most flow conditions the gas would rise through the more viscous mud faster than it would in water. A description of the flow characteristics is developed in terms of the Zuber–Findlay relationship for both pipe and annular flow geometries.

Key Words: two-phase, non-Newtonian fluid, co-current flow, pipe, annulus, void fraction distribution, local velocity distribution

1. INTRODUCTION

When drilling for hydrocarbons the threat of encountering an unexpected high-pressure gas reservoir is ever present. The influx of high-pressure gas into a well is known as a gas kick. If the influx of gas is not detected and checked early enough then the light gas will rise up the wellbore displacing the heavy drilling mud. This will reduce the pressure at the bottom of the well still further, increasing the gas influx rate, which can result in a blowout and complete loss of the well and rig or personnel.

A comprehensive mathematical model of the wellbore fluid mechanics through the development of a gas kick and its control phase has been developed by Schlumberger Cambridge Research (SCR) in association with British Petroleum International. In order to ensure the accurate modelling of the free gas behaviour a comprehensive experimental study has been made into the two-phase flow characteristics which will occur in a well while drilling. The tests were made using a full-scale flow loop and fluids with rheologies representative of field fluids. This paper presents some of the results of the tests together with the conclusions which can be drawn from the investigation.

Previous to the experimental study reported here some correlations existed in the literature for two-phase flow in circular pipes (usually small diameter) and annuli. Only very limited data was available for multiphase flows of non-Netwonian fluids. A review of the relevant data which was previously available is presented in section 2.

The experimental tests were carried out using a 200 mm dia, 12 m long pipe. In order to

†Present address: Sedco Forex, P.O. Box 590, 50 Avenue Jean Jaures, 92542 Mont Rouge Cedex, France.

model the effect of the drill string in the hole an 89 mm dia centre-body was mounted in the centre of the pipe. The experimental facility is discussed in detail in section 3, while details of the instrumentation used are discussed in section 4.

A typical drilling mud can be characterized as having a yield stress and being shear thinning, similar in rheology to non-drip paint. For operational reasons it was not possible to use a genuine drilling mud as the liquid phase, so a suitable alternative had to be identified. The required specification for the fluid together with the selection procedure are discussed in section 5. The term "mud" will be used throughout this paper to describe this fluid.

The data analysis and presentation techniques are given in section 6.

In order to identify accurately the effects of each of the dependent parameters, it is necessary to first identify the characteristics of the facility. These tests were carried out using air–water flows, they included measuring the local flow parameters and the spatially-averaged flow characteristics. They are discussed in section 7.2.

The results of the gas–mud experiments are presented for the pipe geometry in section 7.3. Comparison between the results for gas–water flows, which are the basis of the gas rise models used in most existing kick simulators, and the gas–mud flows show some quite striking differences. Unlike the air–water flows where there is a continuous distribution of bubble sizes, in the mud there is a bimodal distribution, consisting of very small bubbles which are held in suspension and large bubbles which propagate very quickly. The gas rise velocity is much larger for air–mud flows than for similar flow conditions for air and water, despite the higher viscosity.

2. GAS–LIQUID FLOWS

Flow pattern maps like those of Duns & Ros (1963) are often used to characterize multiphase flow regimes and their associated bubble rise velocities. The flow regimes and the transitions between the different patterns are determined by subjective observation of experimental tests. These maps have been used in a number of multiphase flow models, such as that of Aziz *et al.* (1972). The difficulty in applying these models to large scale oil field applications is that the flow pattern maps are usually based on tests in small-diameter pipes with Newtonian fluids.

Some limited work has been carried out in large-pipe geometries. Nakagawa & Bourgoyne (1989) reported tests made with air and water which used a 15 m long 152 mm pipe with a centre-body. Unfortunately, the level of scatter in the experimental data makes is difficult to draw any realistic conclusions from the results. Rader *et al.* (1975) looked at the rise of gas swarms injected at the bottom of a 2000 m deep vertical well but had little control on the gas injection conditions, making the data very difficult to interpret.

A number of authors, notably Zuber & Findlay (1965), have taken a more theoretical approach. They showed that the bubble rise velocity was dependent upon not only the relative velocity between the two phases but also the relation between the bubble concentration profile and the liquid velocity profile. This latter phenomenon can be highlighted by a situation where the bubbles were concentrated in the centre of the pipe where the liquid velocity was greater than the mean flux, thus enhancing the bubble convection velocity. A theoretically-based correlation to model this phenomena was derived by Zuber & Findlay (1965). In this model the mean gas velocity, v_G, is given by

$$v_G = C_0 v_h + v_{rel}, \qquad [1]$$

where C_0 is a constant, v_{rel} is the gas bubble relative velocity and the homogeneous velocity, v_h, is defined as

$$v_h = v_{GS} + v_{LS} = \frac{Q_G}{A} + \frac{Q_L}{A}; \qquad [2]$$

v_{GS} and v_{LS} are the gas and liquid superficial velocities, respectively, A is the cross-sectional area of the flow and Q_G and Q_L the volumetric flow rates.

Zuber & Findlay (1965) were not the first to propose a relationship of this form, but they were

the first to give it some theoretical justification. They proposed that the coefficient C_0 was related to the distribution of bubbles and their relative velocities across the pipe. They showed that

$$C_0 = \frac{\overline{v_L^* \epsilon^*}}{\overline{v_L^*}\,\overline{\epsilon^*}}, \quad [3]$$

where

$$\bar{x} = \frac{1}{A}\int_A x \, dA; \quad [4]$$

v_L^* is the local velocity and ϵ^* is the local void fraction. It is clear that if both of the velocity and void fraction profiles are peaked and the peaks coincide then $C_0 > 1.0$. If, however, the peaks occur at different points in the pipe then $C_0 < 1.0$. If either of the profiles are flat then $C_0 = 1.0$. By suggesting plausible centre-peaked bubble concentration profiles Zuber & Findlay (1965) suggested that C_0 would lie in the range 1.0–1.5. A value of $C_0 = 1.2$ was recommended as being most appropriate.

Although is is widely reported, notably Van der Welle (1985), that bubbles will propagate towards the centre of a pipe, giving a centre-peaked profile, there is some literature, notably Sekoguchi *et al.* (1981) and Herringe & Davis (1976), that shows that at low mean void fraction levels wall-peaked bubble concentration profiles can exist. If these voidage profiles exist in a flow regime where the liquid velocity profile has a centre peak, then the coefficient $C_0 < 1.0$.

There is a large volume of published literature which examines the void fraction profiles in multiphase flows. This has been reviewed by Johnson *et al.* (1990).

The rise velocity of a bubble in a stagnant media, v_{rel}, is a critical parameter in the "Zuber–Findlay" model, [1]. The behaviour of these bubbles has been studied by many authors, and will be discussed briefly here. Wallis (1969) assumed Stokes flow both around and inside the bubble and this approach was carried further by Govier & Aziz (1982). In air–water flows, this approach is limited to bubbles of <2 mm dia. Harmathy (1960) developed a correlation for experimental data to describe the rise of single, slightly larger, bubbles as a function of density difference and surface tension. This correlation, which is independent of bubble size, gave

$$v_{rel} = 1.53\left[\frac{g(\rho_L - \rho_G)\sigma}{\rho_L^2}\right]^{1/4}, \quad [5]$$

where ρ_L and ρ_G are the liquid and gas densities, respectively, g is the acceleration due to gravity and σ is the interfacial tension. For air and water, at 1 bar pressure, this predicts a bubble velocity of 0.25 m/s.

We can define the mean gas void fraction, $\bar{\epsilon}$, as

$$\bar{\epsilon} = \frac{\text{Volume occupied by gas in test cell}}{\text{Total volume of test cell}}. \quad [6]$$

As $\bar{\epsilon}$ increases, an individual bubble will rise less quickly as it will be hindered by other bubbles. An equation to describe this process was derived by Zuber & Hench (1962), who showed

$$v_{rel} = v_{rel0}(1 - \bar{\epsilon})^c, \quad [7]$$

where v_{rel0} is the relative velocity of an isolated bubble and c is a constant in the range 0–3 dependent upon the bubble size, a value of 1.5 was recommended for air and water. The value of 1.5 was also theoretically derived for solid spheres by Kowe *et al.* (1988).

For larger bubbles, where the bubble is sufficiently large to fill the pipe, the relative velocity is limited by the rate at which the liquid phase will fall past the gas. Davis & Taylor (1950) considered inviscid flow around the nose of the bubble in order to evaluate v_{rel}. They derived the equation

$$v_{rel} = 0.35\sqrt{\frac{g(\rho_L - \rho_G)D}{\rho_L}}, \quad [8]$$

where D is the diameter of the pipe. This is normally referred to as the "Taylor" bubble velocity. It is based on the curvature of the nose of the bubble using the pipe diameter as the scaling parameter, so [8] will only apply to the flow in a pipe and not an annulus. A number of authors,

notably Rader *et al.* (1975) and Barnea & Shemer (1986), examined "Taylor"-type bubbles rising in annuli. They found that the bubbles would wrap almost entirely round the centre-body but would leave a path for the liquid to flow past the bubble, enabling the bubbles to rise faster than in a pipe. The latter authors suggested a modification of the "Taylor" bubble velocity, substituting an effective diameter, D_{eff}, into [8], based on the mean of the gap width and the gap circumference, hence:

$$D_{\text{eff}} = \frac{1}{2}\left[\frac{\pi(D_o + D_i)}{2} + \frac{D_o - D_i}{2}\right]; \quad [9]$$

D_i and D_o are the inner and outer annular diameters, respectively.

For the geometric configurations tested here with air and water flowing in a pipe the "Taylor" bubble velocity would be 0.49 m/s, while in the annulus the velocity is 0.55 m/s.

It is clear that two of the dominant parameters affecting the gas relative velocity are the bubble size and the local void fraction distribution in the pipe. There is a large amount of contradictory evidence in the literature describing the effect of these two parameters in gas–water flows. This has been discussed in detail by Johnson *et al.* (1990). It is clear that the developed flow can be a function of the gas injection conditions. It is desirable, therefore, when designing an experimental test facility that the rig is designed to minimize the effects that the injection conditions will have on the flow which is being studied.

3. EXPERIMENTAL FACILITY

The two-phase flow loop (Mud loop) used for the tests discussed in this paper forms part of the multiphase flow test facilities at SCR, figure 1. In the present test configuration it has been used for gas–liquid flows, although solid–liquid and liquid–liquid flows can also be evaluated. The facility offers a straight flow length of almost 12 m, 9.5 m of which is transparent to permit visual evaluation of the flows. It is mounted on a 15 m long table which can be pivoted, enabling tests to be carried out in all orientations from horizontal to vertical. It has been designed to permit tests of Newtonian and non-Newtonian fluids and also shear degradable liquids without damage to either the fluid or the facility. This makes it suitable for studying drilling muds, cements and fracturing or production fluids, together with gas or solids transport. The facility is designed to operate at pressures of up to 10 bar.

The Mud loop working section comprises 5 perspex pipe sections with the instrumented test section at the top. It has a flow development length of 8.5 m or 42.5 pipe diameters. It is possible to test two flowing geometries. The *pipe* geometry has a circular cross section of 200 mm dia. In order to model the condition of flow around a drill string an *annular* geometry with an 89 mm dia centre-body can be used. Stainless steel plenum chambers are fitted onto each end of the loop.

The physical arrangement of the liquid and gas injection system is shown in figure 2. The liquid phase is introduced into the 200 mm i.d. plenum chamber, through a 150 mm supply line. The gas is introduced into the plenum chamber through 8, 10 mm dia injectors. The two-phase flow then passes through a Mitsubishi flow straightener and into the flow development zone. The flow straightener is used to homogenize the flow and generate small bubbles, in order to simulate the flow which would be expected in a well where the influx would be through small pores or fractures. The specification of the injection system is discussed in more detail by Johnson *et al.* (1990).

A schematic view of the fluid flow paths to and from the mud loop is shown in figure 3. The air supplied to the loop by two Compair compressors with a total capacity of 1700 m^3/h at a delivery pressure of 7 bar. The flow is controlled by a Varipack microflow needle valve for flows ($Q_G < 25\ m^3/h$) or a Camflex valve for larger flow rates.

The fluid storage is in 4 tanks, of volume 4–8 m^3. The fluid storage tanks are interconnected to permit the flow to be returned to one tank while fluid is drawn from another. This permits settling time for de-aeration of the liquid when viscous fluids are tested.

The fluid is pumped by a PCM mono-type pump, capable of flowing 240 m^3/h against a head

of 6 bar. The mono pump was chosen as it is a low-shear device and will not cause shear degradation to the fluids tested in the facility. The fluid is pumped through 50, 100 or 150 mm pipes, dependent upon the volumetric flow rate, then a 150 mm flexible line onto the inclinable table. A throttle valve has been mounted on the end of the return line to permit dynamic pressure control of the entire facility.

The experimental test conditions are summarized in table 1.

Figure 1. Photograph of the multiphase flow test facility at SCR, the mud loop is shown in the right-hand side with the three-phase loop on the left.

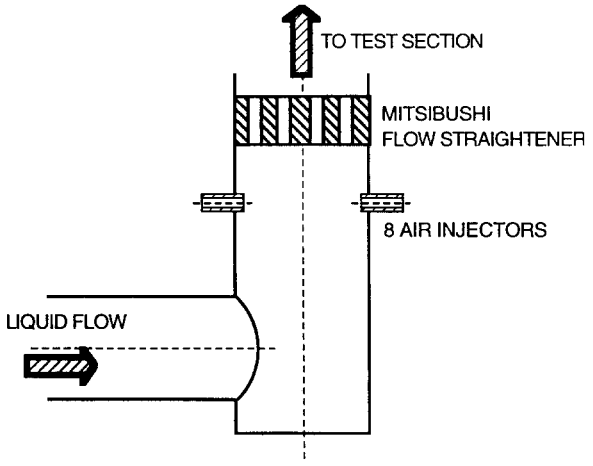

Figure 2. Schematic view of the plenum chamber showing liquid flow and air injection paths. Also, the Mitsubishi flow straightener at the top of the chamber.

4. INSTRUMENTATION

Measurements made during an experiment include the liquid and gas flow rates, the absolute pressure in the test section, the differential pressure along a length of the test section and the local void fraction and gas bubble velocity. A photograph of the instrumented test section is shown in figure 4. To ensure accuracy, regular calibration checks are carried out on all instrumentation.

The differential pressure measurement was made along a known length of the test section using a Honeywell differential pressure transducer with the remote rescaling facility using a smart field controller. This was found to be invaluable as the transducer could be rescaled remotely while physical access to the instrumentation was denied. The accuracy of these devices is rated as $\pm 0.1\%$ of the full scale, this was confirmed with regular calibration checks. The transducer was linked to test section pressure tappings with flexible lines filled with de-ionized water. To eliminate the problem of contamination of the pressure tapping with flow loop fluids the lines were bled regularly.

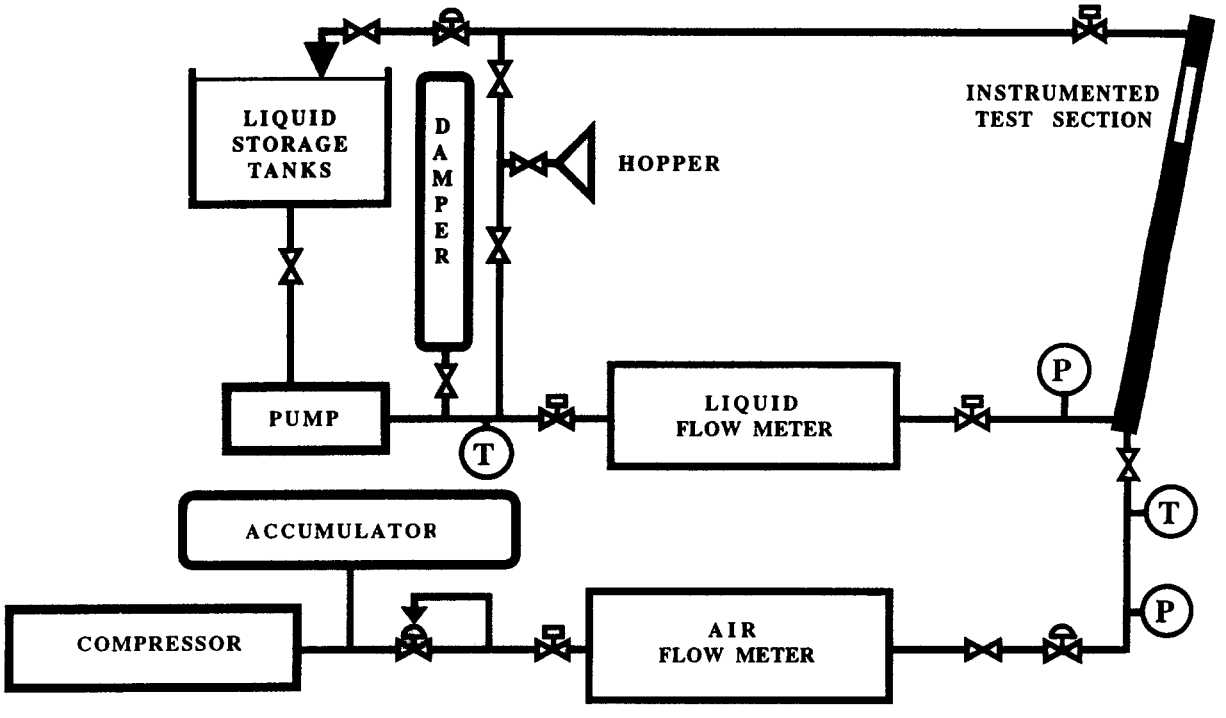

Figure 3. Schematic view of the fluid flow path to and from the mud loop.

Table 1. Experimental test conditions

Liquid Newtonian	Water
Liquid non-Newtonian	Xanthum gum solution
Gas	Air
Pipe length	12 m
Pipe i.d.	200 mm
Centre-body o.d.	89 mm
Operating pressure	1.0 ± 0.5 bar
Operating temperature	20 ± 10°C
Liquid superficial velocity	0.25 – 1.6 m/s
Gas superficial velocity	0.03 – 2.0 m/s

The absolute pressure was measured in the test section using a Validyne gauge pressure transducer, rated to ± 1 bar with an accuracy of 0.5%.

The air flow measurement was made using two-wire linear mass flow meters. These devices measure the mass flow of the gas using two heated platinum coils placed in the flow to an accuracy of 1% of reading. Being mass-flow-sensitive, only a single measurement needs to be taken with no absolute pressure correction at this point.

Three electromagnetic flow meters with ranges 0–50, 0–100 and 0–200 m^3/h are used for the liquid flow measurement. This type of device will maintain its calibration for viscous Newtonian and non-Newtonian fluids as well as water, although they can only be used with electrically-conducting fluids. These devices have an accuracy of $\pm 0.25\%$ of full scale. In the pipe geometry this is equivalent to an uncertainty of ± 1.1, 2.2 or 4.4 mm/s, dependent upon which flow meter is used.

The local void fraction and bubble velocity were evaluated using radio frequency (RF) probes. These instruments are described in detail by Vigneaux *et al.* (1988), and will only be discussed briefly here. The measuring device is a small coaxial probe connected to a high-frequency (1–2 GHz) bridge circuit. It is sensitive to the difference in the dielectric constant between air and water, and therefore acts as a bubble detector. The local void fraction can be derived from the fraction of time when the probe is in air.

In the physical arrangement used for the tests, two probes were mounted with their sensing volumes in line with the flow but 10 mm apart. By using auto- and cross-correlation of the two signals it is possible to estimate the time-averaged bubble velocity and size. The probes were traversed across the pipe using a stepper motor and a screw thread drive mechanism, controlled by a BBC microcomputer. Data was collected on a vertical plane across the pipe diameter.

The kernel of the data collection system is an Apple Macintosh II (MAC) personal computer, which runs the LABVIEW data acquisition package. This collects all of the data, down-loaded from various satellite devices via IEEE or RS232 interfaces.

The data acquisition system used with the facility is shown schematically in figure 5. The analogue signals from the flow meters and the pressure transducers are transmitted to a Nicolet 4094A digital oscilloscope. Following the completion of the data collection period the digitized data is down-loaded to the MAC via an IEEE interface.

The raw signals from the RF probes are fed into a Solatron 1200 signal processor where cross-correlation is used to calculate the bubble velocity, the processed data is then fed to the MAC via the IEEE interface. The void fraction is calculated directly from the RF probe analogue signals by calculating the amount of time that the probe is in air. This data is transferred to the BBC microcomputer, which is also used to control the transverse mechanism, then onto the MAC via the RS232.

5. FLUID RHEOLOGY

The criteria for the selection of a fluid for the tests was that the fluid should match the rheology of typical drilling fluids and it should be non-abrasive. A drilling mud has a yield stress to prevent drilled cuttings from sinking down the wellbore when pumping is suspended. They are also shear thinning to reduce pumping power and surface pressures while circulating. Figure 6 shows the

rheogram for a typical drilling mud described by Dairanieh & Lahalih (1988) as suitable for a 1500–2500 m deep well.

The fluids used for these tests were two aqueous xanthum gum solutions and water. The first polymer solution, fluid A, was a 5.0% by wt aqueous solution of a proprietary polymer known as IDVIS. The second solution, fluid B, was nominally a 0.2% solution of the same polymer. A rheogram showing the rheology of both polymer solutions and water is shown in figure 6. The

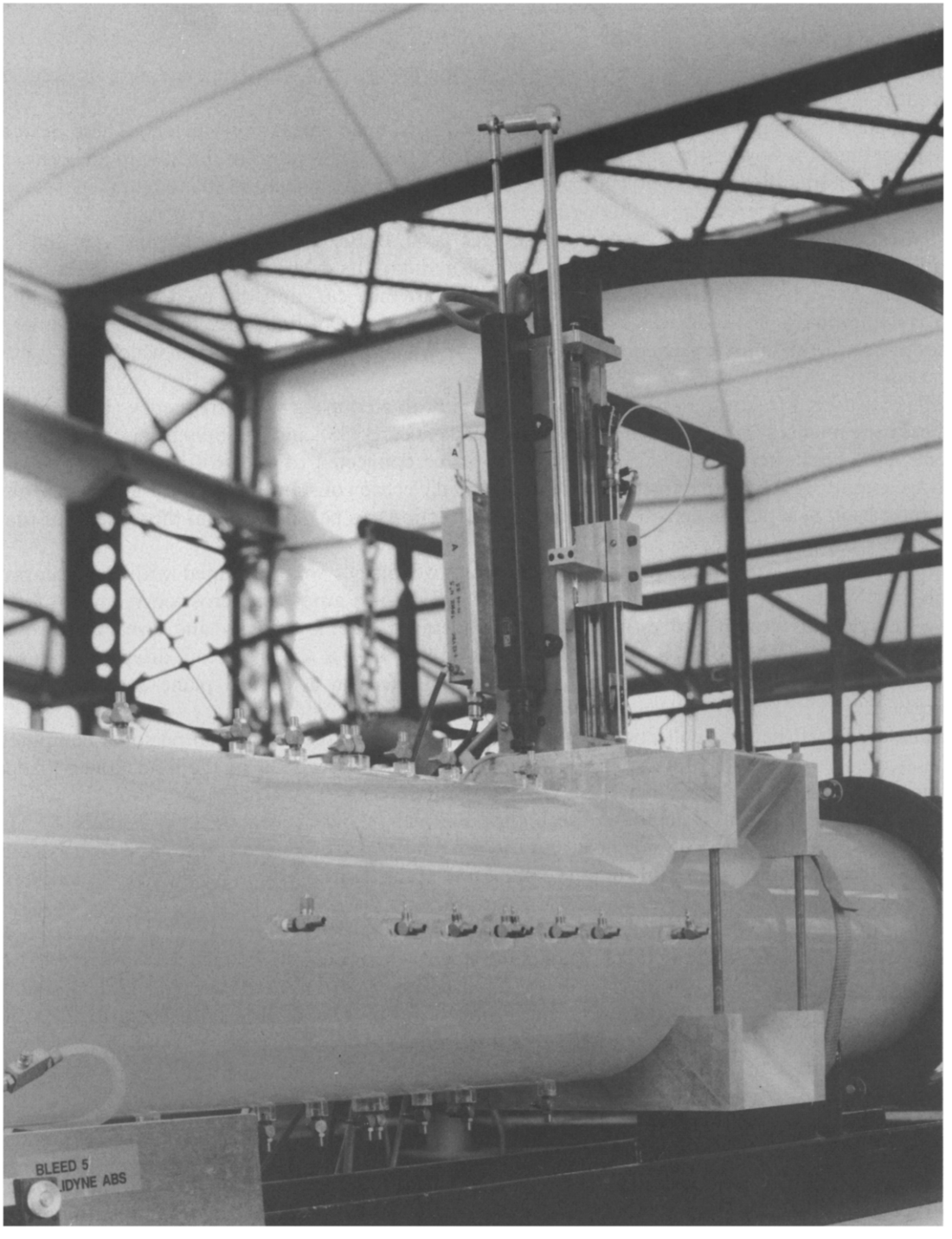

Figure 4. Photograph showing the instrumented test section. The pressure tappings can be seen on the side of the pipe, with the RF probe traverse mechanism mounted on top.

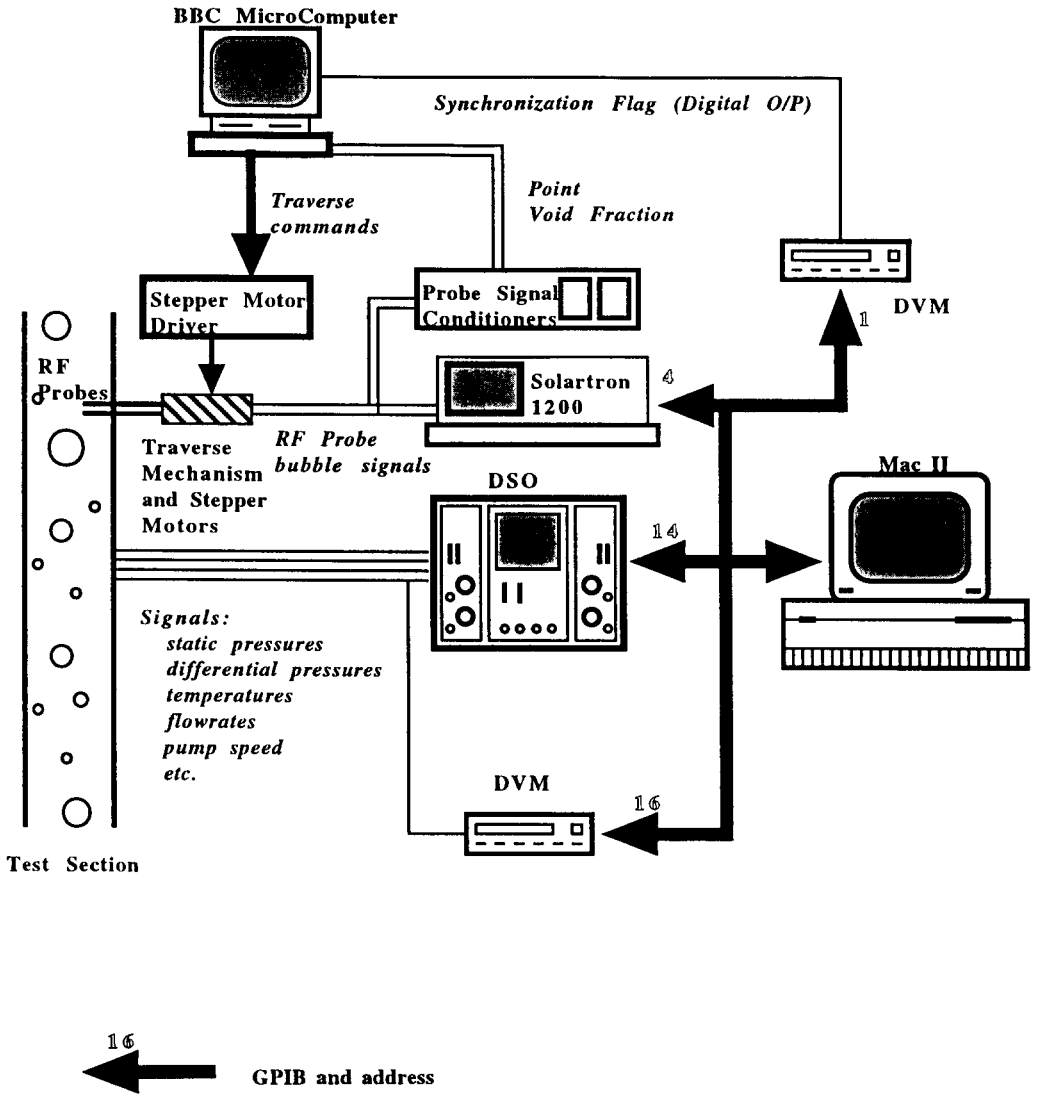

Figure 5. Schematic view of the data acquisition equipment used for the tests.

rheology of mud A is very similar to the rheology of the drilling mud, while mud B is much less viscous. A Herschel–Buckley rheology model was applied to the polymer solutions, the resulting models were:

for fluid A,

$$\tau = 4.0 + 0.72 \cdot \dot{\gamma}^{0.40}, \qquad [10]$$

where τ was the shear stress and $\dot{\gamma}$ was the shear rate;

and

for fluid B,

$$\tau = 1.33 + 0.30 \cdot \dot{\gamma}^{0.47}. \qquad [11]$$

Xanthum gum solutions are prone to bacteriological attack which can degrade the fluid rheology in a period of 24 h. To avoid this scenario a proprietary biocide was used with a large *kill* dose (2000 ppm) followed by regular weekly booster doses (500 ppm). The fluids were regularly checkedand it was found that the rheology of the solutions would remain unchanged for periods >4 months of regular usage.

6. DATA PRESENTATION

The spatially-averaged parameters recorded during the tests are the liquid volumetric flow rate, Q_L, the gas mass flow rate, $\dot{m}_G$, the test section absolute pressure, p_{abs}, and the differential pressure along a length of the test section, Δp, and the mud temperature, T. The experimental results are presented in the form of the gas velocity, v_G, the homogeneous velocity, v_h, and the mean void fraction, $\bar{\epsilon}$. The gas volumetric flow rate, Q_G, is derived from the ideal gas equation, assuming that the gas temperature in the test section is at equilibrium with the mud. The homogeneous velocity is calculated from [2] and the average gas velocity is calculated from

$$v_G = \frac{Q_G}{\bar{\epsilon} A}. \quad [12]$$

The differential pressure measured with the transducer is not a direct measurement of the void fraction, as there is a contribution to the Δp from the frictional pressure drop along the pipe wall and the difference in density between the liquid in the pipe and that in the bleed lines. If acceleration terms and the gas density are neglected, the vertical momentum balance gives

$$\bar{\epsilon} = \frac{\Delta p - \Delta p_{fric}}{\rho_L g l} - \epsilon_{bck}, \quad [13]$$

where Δp_{fric} is the frictional pressure drop along the pipe and ϵ_{bck} is the void fraction measured with no flow in the pipe normally referred to as the background void fraction; it accounts for the difference in density between mud and the blend line fluid, and any gas bubbles which are held in suspension in the mud by the yield stress.

It is clear that to gain an accurate measurement of the void fraction it is necessary to know the frictional pressure drop along the pipe wall. The approach taken for this is to use the two-phase frictional pressure drop correlation derived by Friedel and reported by Whalley (1987). This gives

$$\frac{\Delta p_{fric}}{l} = \phi^2_{L0} \left[\frac{dp}{dz}\right]_{L0}, \quad [14]$$

where ϕ^2_{L0} is a function of the flow parameters and $dp/dz|_{L0}$ is the single-phase frictional pressure gradient for the liquid phase with the same mass flow rate as the total two-phase mass flow rate. The single-phase friction factor is calculated from the Reynolds number using a relation evaluated in experimental tests with a single-phase liquid flow. These tests are discussed in detail in a later section.

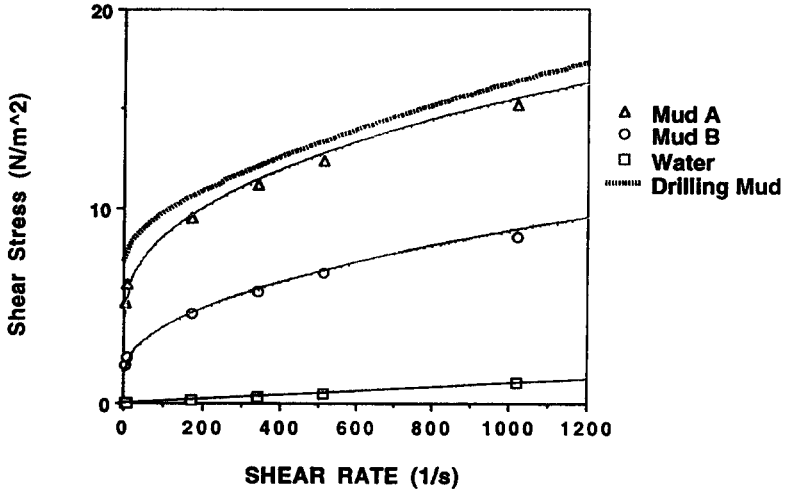

Figure 6. Rheogram showing the rheology of a typical drilling mud from Dairanieh & Lahalih (1988). Also, the two polymer solutions (fluids A and B) and that of water together with the Herschel–Buckley models are shown for the fluids.

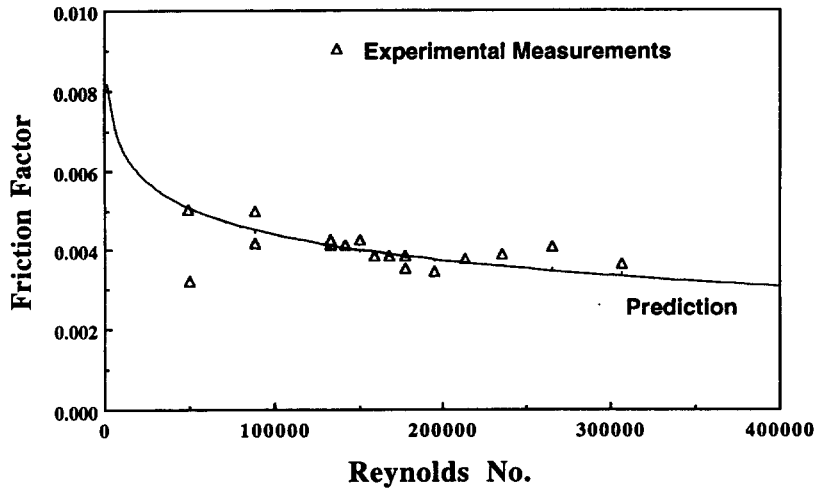

Figure 7. Graph showing the dimensionless friction factor, f, vs Reynolds number, Re, for single-phase water flow in a pipe geometry, also the prediction from [25].

In single-phase Newtonian liquid pipe flow the definition of the Reynolds number is

$$\mathrm{Re} = \frac{\rho v D}{\mu}, \qquad [15]$$

where v is the fluid velocity, μ is the appropriate fluid viscosity and D is the pipe diameter. For non-Newtonian annular fluid flow the viscosity is variable and the pipe diameter is no longer the principal dimension. A generalized definition of Re is

$$\mathrm{Re} = \frac{\rho v D_{\mathrm{eff}}}{\mu_{\mathrm{eff}}}, \qquad [16]$$

where

$$\mu_{\mathrm{eff}} = \frac{\tau_0}{\dot{\gamma}_{\mathrm{eff}}} + k\dot{\gamma}_{\mathrm{eff}}^{n-1}. \qquad [17]$$

The appropriate value of $\dot{\gamma}_{\mathrm{eff}}$ for pipe flow is

$$\dot{\gamma}_{\mathrm{eff}} = \frac{6v}{D}, \qquad [18]$$

as shown by Skelland (1967). For annular flow with Newtonian fluids, D_{eff} is calculated from

$$D_{\mathrm{eff}} = 0.6870 \cdot (D_{\mathrm{o}} - D_{\mathrm{i}}), \qquad [19]$$

as shown by Jones & Leung (1981).

For multiphase flow the Reynolds number is calculated using the mixture density and the homogeneous velocity, hence

$$\mathrm{Re} = \frac{\rho_{\mathrm{m}} v_{\mathrm{h}} D_{\mathrm{eff}}}{\mu_{\mathrm{eff}}}. \qquad [20]$$

The background void fraction was evaluated with a stationary column of test liquid in pipe.

The RF probes will yield a measure of the local void fraction ϵ_* and the local gas bubble velocity

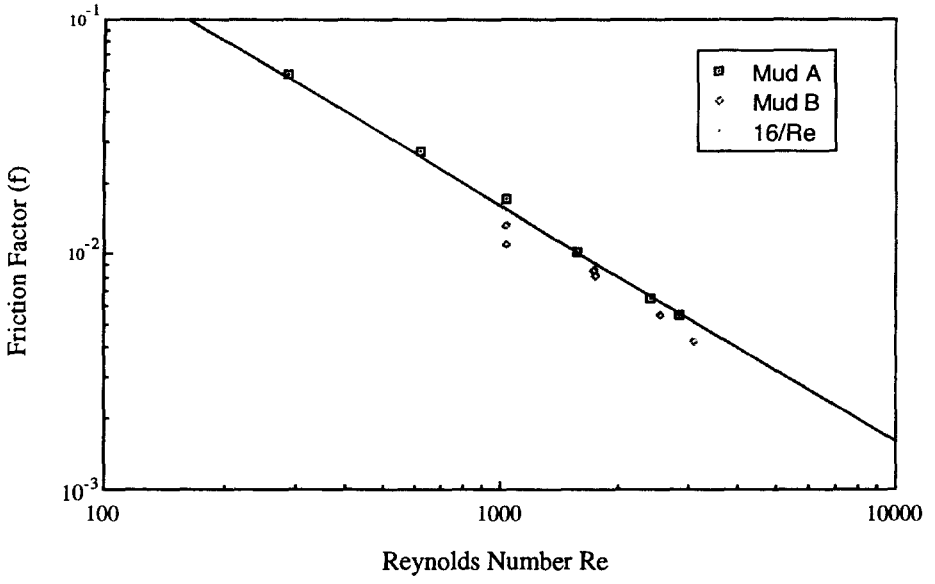

Figure 8. Graph showing the dimensionless friction factor, f, vs Reynolds number, Re, for single-phase mud flow in the pipe geometry, also the prediction from [27].

v_{G*}. It is possible to calculate the spatially-averaged void fraction from the locally-measured RF probe data using

$$\langle \epsilon \rangle = \frac{1}{A} \int_A \epsilon_* \, dA, \qquad [21]$$

where A is the pipe cross-sectional area.

All data inferred from the RF probe results will be denoted with the symbols $\langle\ \rangle$. It is also possible to calculate the average gas velocity from the locally-measured data using

$$\langle v_G \rangle = \frac{\frac{1}{A} \int_A \epsilon_* v_{G*} \, dA}{\frac{1}{A} \int_A \epsilon_* \, dA}. \qquad [22]$$

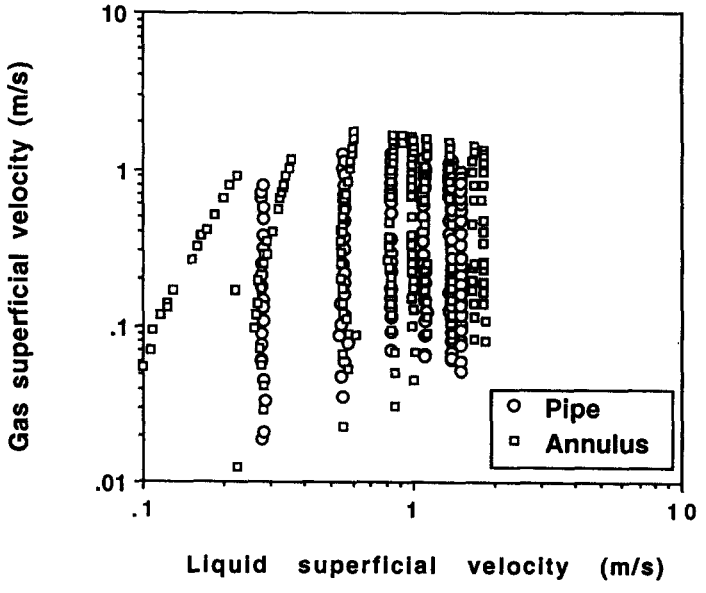

Figure 9. Graph of liquid and gas superficial velocities for air–water tests in pipe and annular geometries.

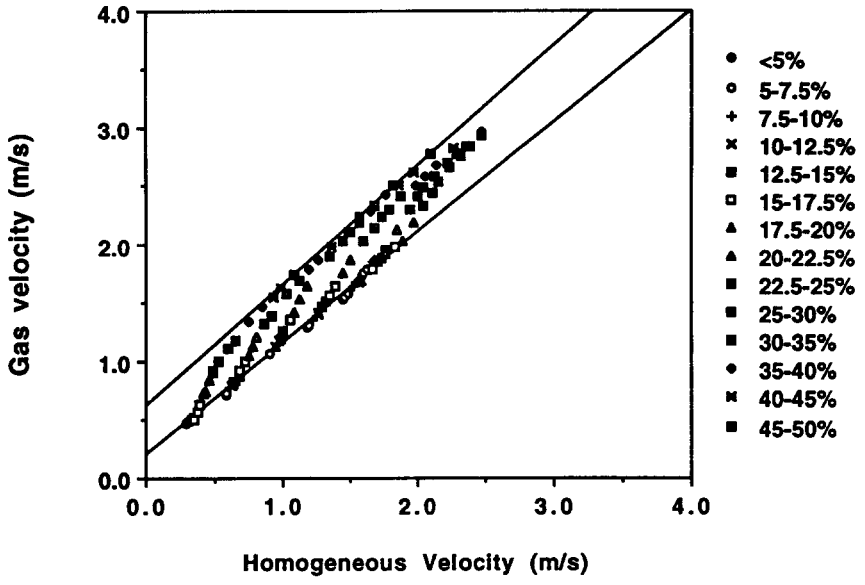

Figure 10. Zuber–Findlay plot for air–water flows in the pipe geometry.

This data can be compared directly with the mean void fraciton $\bar{\epsilon}$ and the mean gas velocity v_G derived from the differential pressure measurements.

Zuber & Findlay (1965) showed that the coefficient C_0 could be expressed as

$$C_0 = \frac{\frac{1}{A}\int_A \epsilon_* j_* \, dA}{\frac{1}{A}\int_A \epsilon_* \, dA \frac{1}{A}\int_A j_* \, dA}, \quad [23]$$

where j_* is the local volume flux which can be defined as

$$j_* = v_{G*} - v_{rel*}. \quad [24]$$

It is possible to calculate a value of C_0 from the void fraction distributions and the bubble velocities measured with the RF probes. We must, however, define a function for the gas bubble relative velocity. There is a large amount of literature available on this subject which is discussed in section 7.2, unfortunately there is no reliable data which covers flows in such large pipes. For the purpose of this test, therefore, we used a correlation taken from the spatially-averaged data presented in section 7.2.1.

7. EXPERIMENTAL RESULTS

7.1. Frictional Pressure Drop Tests

As has been discussed previously, in order to calculate the void fraction it is necessary to have an accurate measurement of the frictional pressure drop along the length of the pipe. Frictional pressure drop tests were made for single-phase liquid flows. The purpose of these tests were two-fold. Primarily it was necessary to measure the friction factor for the geometries and fluids which we were testing. Also, as the signal amplitudes for these tests were much smaller than those for the two-phase flows we would evaluate, it was an excellent opportunity to sort out all of the signal noise problems.

The results for the tests are presented in figure 7 for the water flow in the form of the non-dimensional friction factor vs the Reynolds number. The water flow is entirely turbulent, with the Reynolds number ranging from 10,000 up to 1,000,000. The results, shown in figure 7, have been compared with the prediction of the friction factor in turbulent pipe flow by Moody, reproduced by Massey (1983):

$$f = 0.001375\left[1 + \left(20{,}000\frac{k}{D} + \frac{10^6}{\mathrm{Re}}\right)^{1/3}\right], \quad [25]$$

where k is the surface roughness although the pipe is assumed to be smooth, hence

$$\frac{k}{D} = 0. \quad [26]$$

It should be noted that the largest frictional pressure drop measured during these tests was equivalent to a head of 5 mm of water. The agreement with [25] is good, giving confidence in the use of this approximation as the liquid-phase frictional pressure drop correlation in the calculation of void fraction.

For both of the mud fluids the flow appeared to be almost entirely laminar. We used the Herschel–Buckley Reynolds number, Re, as defined in [16]. The data, figure 8, shows good agreement with the laminar flow equation

$$f = \frac{16}{\mathrm{Re}}, \quad [27]$$

although the Re was as high as 3000. Govier & Aziz (1982) show that transition occurs at a Re $\sim$ 2100, as with Newtonian fluids. However, they report the work of Metzner & Park (1964), who show that transition can be delayed to Re = 10,000 for viscoelastic fluids. The xanthum solutions tested here are very slightly viscoelastic.

The void fraction correction, which is equivalent to the predicted frictional pressure drop, ϵ_{fric}, is fairly small for the air–water flows, up to approx. 0.5%. For the air–mud flows, however, it can be as large as 4%. The Friedel correlation used to calculate the void fraction correction, taken from Whalley (1987), [14], is believed to be accurate to $\pm 20\%$. This will not hinder the accuracy of the air–water test results, but it could reduce the resolution of the air–mud results significantly, especially at low void fraction. For this reason no data will be presented for flows with measured void fraction $< 7.5\%$.

7.2. *Air–Water Flows*

The air–water tests were made over a range of liquid and gas flow rates; the superficial velocities are indicated in figure 9.

7.2.1. *Spatially-averaged results*

The results for the experiments carried out with a vertical pipe and annular flows are shown in figures 10 and 11, respectively. "Zuber–Findlay" plots are used where the gas velocity is plotted vs the homogeneous velocity and the data points are grouped into void fraction ranges. It is very

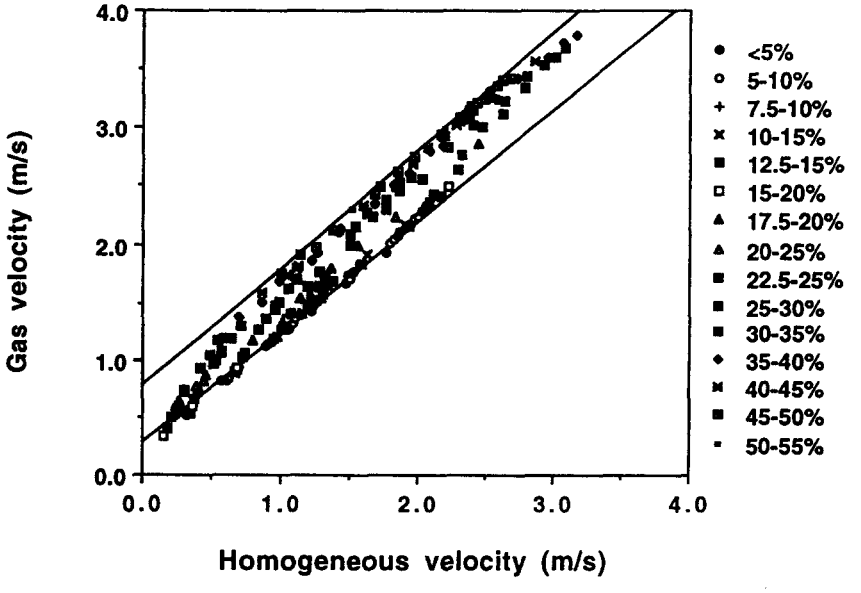

Figure 11. Zuber–Findlay plot for air–water flows in the annular geometry.

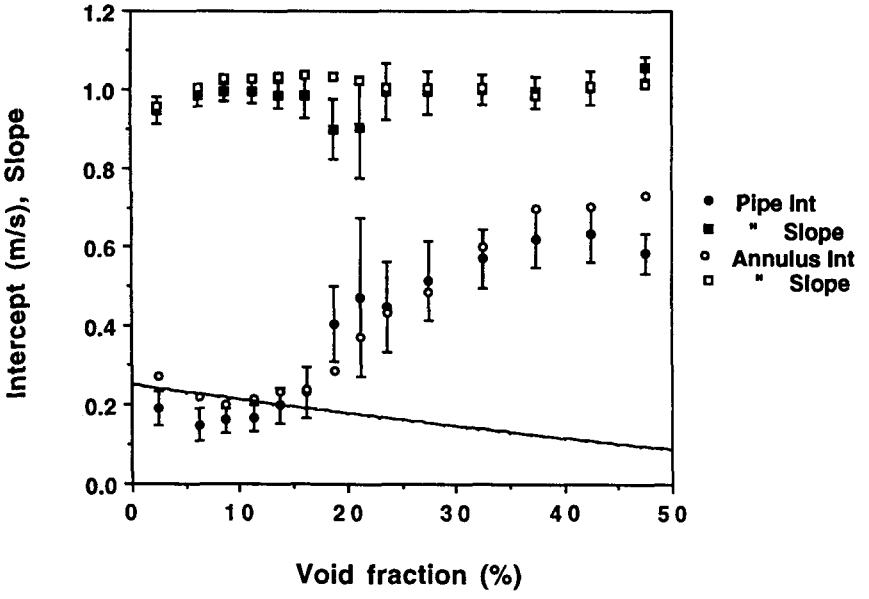

Figure 12. Slopes and intercepts from line fits of the form of [1] for air–water flows in pipe and annular geometries. Also, a line of the form $v_{rel} = 0.25\ (1 - \bar{\epsilon})^{1.5}$.

difficult to draw any conclusions directly from the data presented in this way, so straight-line fits of the form shown in [1] were applied to the different data groups. The resulting intercepts and slopes from the line fits are shown in figure 12. Also shown in this figure are the 95% confidence limits of the straight-line fits for the pipe geometry; the limits for the annular geometry are not shown to avoid confusion, but the amplitudes are approximately the same. In the pipe data the line fits to the results for void fractions between 17.5 and 22.5% appear to be inconsistent with the remainder of the data, suggesting a problem with the experimental results. The amplitude of the confidence limit also indicates this.

The intercept of the line fit can be interpreted as the gas bubble relative velocity, v_{rel}. There appear to be three distinct zones of behaviour of this parameter for both geometrical configurations. For low void fractions, the velocity falls with void fraction indicating a bubbly flow regime. At high void fractions there is a zone of approximately constant v_{rel} with very large bubbles rising up the pipe. These two regimes are linked by a transitional zone.

In the bubbly flow regime, we would expect v_{rel} to vary as in [7], with v_{rel0} given by [5]. A line of the form

$$v_{rel} = 0.25(1 - \bar{\epsilon})^{1.5} \qquad [28]$$

is also shown in figure 12. The data appears to show fairly good agreement with this line, especially that recorded in the annular geometry. This flow regime appears to occur up to a void fraction of approx. 15% for both the pipe and annular flow geometries.

As the void fraction, and hence the bubble concentration, increases the bubbles will agglomerate and form larger bubbles which will have a higher relative velocity. This agglomeration process can be identified in the results (figure 12) by the increase in v_{rel} in the transitional zone.

Table 2. Experimental test conditions for RF probe experiments, together with spatially-averaged void fraction measurements and RF probe integrated data

Run No.	V_{LS} (m/s)	V_{GS} (m/s)	V_h (m/s)	$\bar{\epsilon}$	V_G (m/s)	$\langle\epsilon\rangle$	$\langle V_G\rangle$ (m/s)	C_0
A88	0.288	0.052	0.341	0.088	0.599	0.078	0.584	1.02
A148	1.469	0.647	2.117	0.219	2.957	0.216	2.595	1.03
A149	0.743	0.195	0.938	0.129	1.508	0.107	1.520	1.04
A151	0.650	0.360	1.010	0.212	1.636	0.221	1.664	1.01
A152	0.862	0.088	0.951	0.066	1.333	0.059	1.274	1.02
A153	0.866	0.086	0.998	0.144	1.532	0.096	1.336	1.04

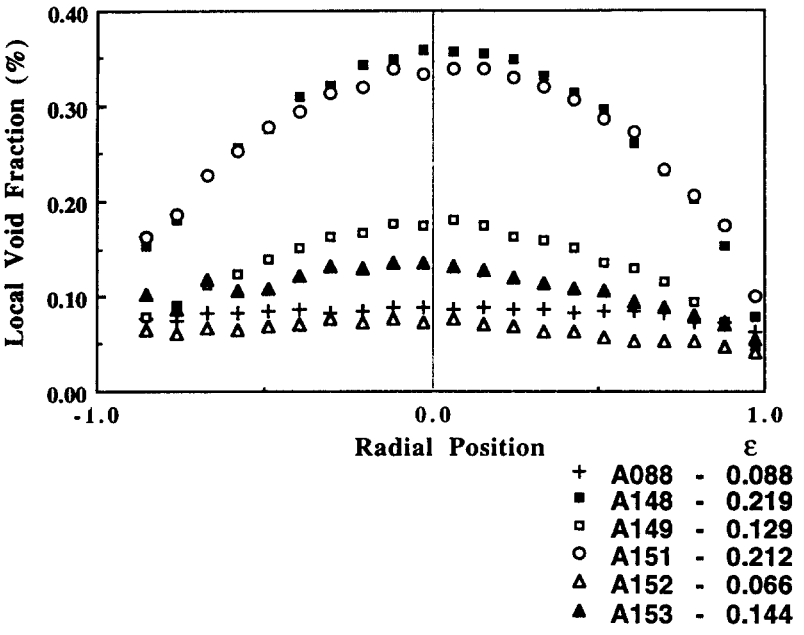

Figure 13. Local void fraction distribution for air–water flows in the pipe geometry.

When the void fraction is very high and the bubbles are sufficiently large to be influenced by the pipe walls then, as with Taylor bubbles, the terminal velocity will be limited by the need for the liquid phase to flow down the pipe around the bubbles. It appears that the limiting velocity for the pipe flow is approx. 0.60 m/s, while for the annular geometry it is approx. 0.70 m/s. In both cases the terminal velocity is larger than the Taylor bubble velocity, [8] and [9]. This is thought to be due to drag reduction from the high level of turbulence introduced by the bubble wakes.

The v_{rel} model used for the analysis of the spatially-resolved data and derivation of C_0 is derived from the relation between the relative velocity and the void fraction found here. We defined v_{rel*} as

$$\epsilon_* < 0.15 \quad v_{rel*} = 0.20 \text{ m/s},$$

$$0.15 < \epsilon_* < 0.35 \quad v_{rel*} = 0.2 + 2 \cdot (\epsilon_* - 0.15) \text{ m/s},$$

$$\epsilon_* > 0.35 \quad v_{rel*} = 0.60 \text{ m/s}.$$

This assumes that at low void fractions ($\epsilon < 10\%$) the gas transport is by small bubbles travelling at 20 cm s^{-1}. For high void fraction ($\epsilon > 35\%$) the gas bubbles are assumed to move at 60 cm s^{-1}. For intermediate void fractions the gas transport is assumed to be transitional between these two bubble flow regimes.

The slope of the line from [1] is a function of the bubble concentration and velocity distribution across the pipe. In the data presented here, figure 12, the slopes of both lines appear to be weakly dependent upon the void fraction. For the bubbly flow regime and the low void fraction end of the transitional flow regime the slope of the lines appears to be approximately constant. For the pipe flow the slope is approx. 1.0, while for the annular geometry it is approx. 1.03. For the higher void fraction flows the slope is approximately unity. These measurements are much lower than those suggested by Zuber & Findlay (1965), who recommended values of 1.2 from small pipe data, implying flatter velocity and void fraction profiles in the larger geometries.

7.2.2. Spatially-resolved results

The experimental test conditions used for the RF probe traverse tests are shown in table 2. The data are presented as the liquid and gas superficial velocities and the homogeneous velocity. The RF probes were not used for the annular tests as it was not possible to traverse them through the centre-body. The results of the local void fraction and gas velocity traversed are shown in figures 13 and 14, respectively.

The results indicate that at low gas rates the void fraction profile is almost completely flat, while at high mean levels it has a very high centre peak. It should also be noted that the profiles are almost completely independent of the homogeneous velocity. The local gas bubble velocity is presented in the normalized form of v_{G*}/v_G. The results suggest that at low void fractions the profile has a high centre peak, while at high gas rates the velocity profile is much less peaked. It is thought that this flattening of the velocity profile is due to the increase of the turbulence level and increase in size of the turbulent structures caused by the larger bubbles.

The results of the void fraction measurements are summarized in table 3. The results for the mean void fraction and gas velocity derived from the differential pressure measurements are shown in table 2 together with the data derived from traverse test results for comparison. The mean void fraction and gas velocity are calculated from [21] and [22]. The agreement appears to be good in all test cases, giving confidence in the experimental techniques.

As was shown above, it is possible to calculate a value for the coefficient C_0 from the spatially-resolved experimental data using [23]. Using the v_{rel} correlation discussed above the coefficient C_0 was evaluated from the experimental data, the results are shown in table 2. All of the predictions lie in the range 1.01–1.04. Whilst they are not exactly equivalent to the values measured from the Zuber–Findlay plots, the agreement is extremely good, giving much confidence in the experimental technique together with the Zuber–Findlay analysis.

7.3. Air–Mud Flows

The superficial liquid and gas velocities for the tests with muds A and B are shown in figure 15. The test parameter space for these tests was slightly smaller than that used in the air–water tests for operational reasons.

7.3.1. Mud A

Visual observations of the two-phase flow regimes demonstrated two very interesting phenomena. Firstly, in spite of the large tank capacity used, the mud was saturated with small ($d < 2$ mm) bubbles, which were held in suspension by the yield stress of the fluid. The volume fraction of these bubbles was measured during each test and is referred to as the background void fraction, ϵ_{bck}. The level of the background void fraction was found to vary between 1 and 2%. In all of the analyses it was assumed that the only effect of these bubbles was to modify the density of the mud. Secondly, it was found that for all but the very small gas concentrations the injected gas would

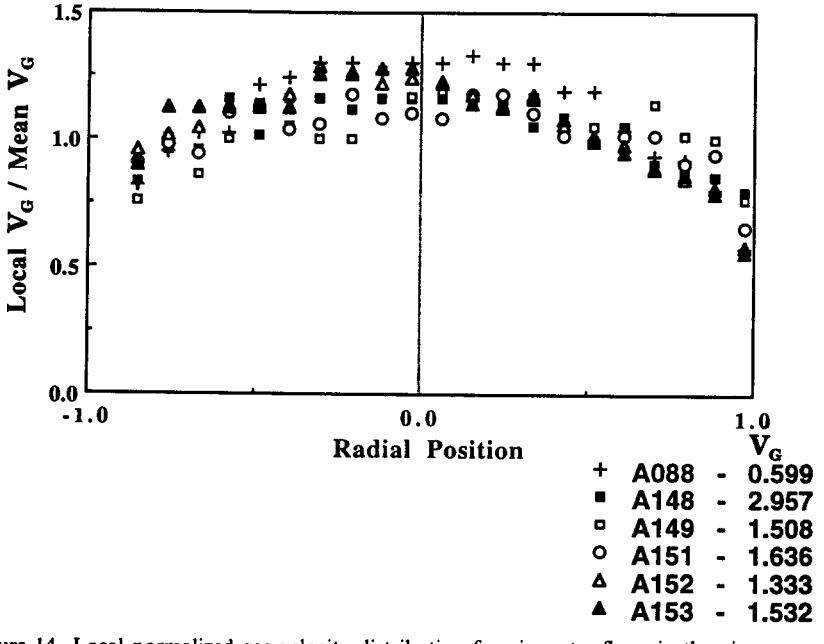

Figure 14. Local normalized gas velocity distribution for air–water flows in the pipe geometry.

Table 3. Summary of results of the RF probe tests

Flow condition	Profile	
	ϵ_*	v_{G_*}
Low $\bar{\epsilon}$	Flat	Peaked
High $\bar{\epsilon}$	Peaked	Flat

rise up the pipe as very large bubbles. The time-averaged void fraction is then determined by the bubble frequency rather than the bubble size.

The performance of the RF probes was significantly impaired by the small bubbles held in the mud by the yield stress. As these bubbles passed through the measuring volume they would increase the level of background noise on the probe signal and make interpretation with the current hardware impossible. Consequently, there were no probe traverse tests reported for the air–mud flows.

As for the air–water data, the results for the air–mud tests are presented in the Zuber–Findlay format, in figure 16; again the test results are separated as bands in void fraction. The amplitude and uncertainty of the frictional pressure drop, with ϵ_{fric} as large as 4%, made it impossible to measure the void fraction with sufficient resolution to calculate meaningful results for void fractions $<7.5\%$. The data for smaller void fractions showed too much scatter to draw any realistic conclusions. This was especially true for flows with larger homogeneous velocities.

For all the void fractions presented the data collapses onto a single straight line on the "Zuber–Findlay" plot, indicating that the gas velocity is independent of void fraction. The line fit gives

$$v_G = 1.35v_h + 0.51. \quad [29]$$

This surprising result is completely at odds with the air–water observations, both here and in other previously published data, where the gas relative velocity was found to be a function of the void fraction. As the relative velocity is constant for all void fractions, this implies that the bubble size is also independent of the void fraction for the flow rates tested. This is consistent with the visual observations that the void fraction was determined by the frequency of the bubbles rather than their size.

This singular large bubble size distribution, in addition to the small bubbles held in suspension by the fluid yield stress, was also noted by Philip *et al.* (1990), who described a bimodal bubble size distribution. The bubble size is dependent upon the balance between the agglomeration and

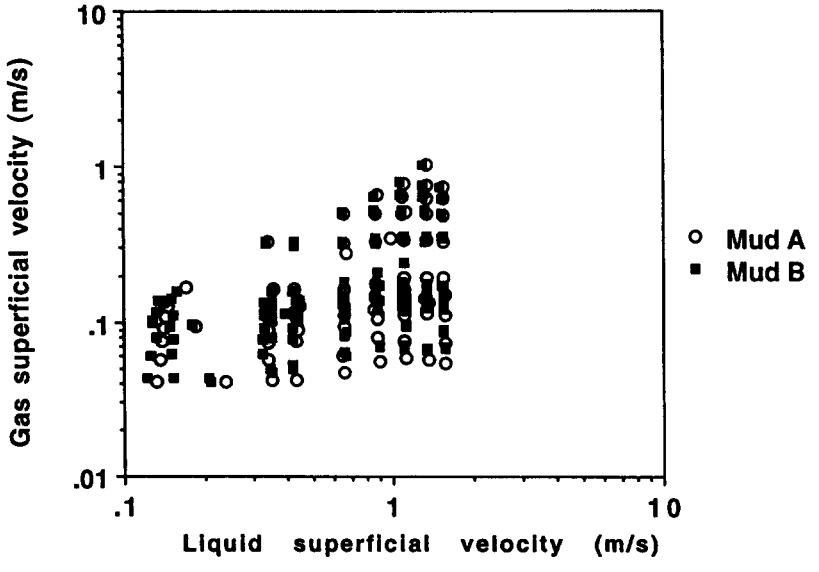

Figure 15. Graph of liquid and gas superficial velocities for air–mud (A and B) tests in the pipe geometry.

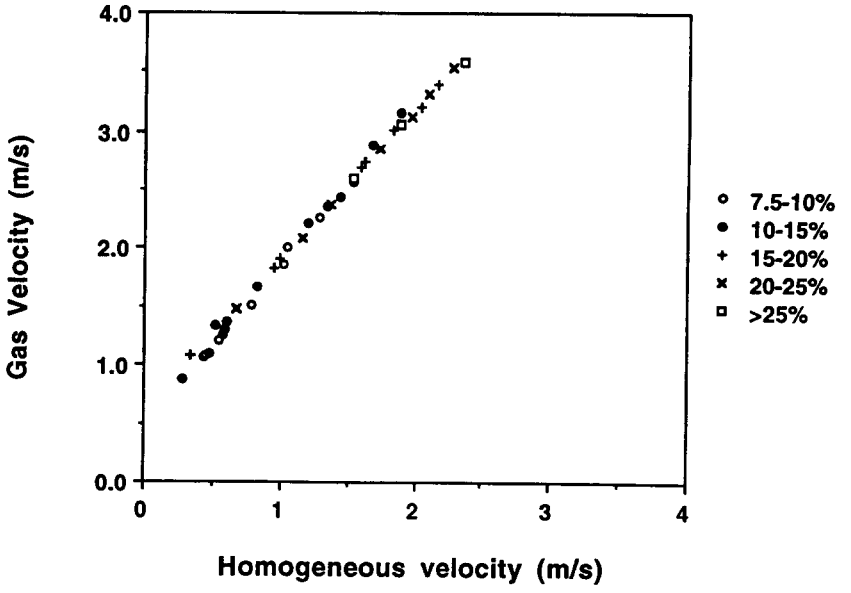

Figure 16. Zuber–Findlay plot for air–mud A flows in the pipe geometry.

the bubble breakup processes. It appears that the bubble breakup process is being inhibited by the increased viscosity of the mud, leaving a larger stable bubble size.

The relative velocity is slightly larger than the "Taylor" bubble velocity for pipe flow, [8], which gives $v_{rel} = 0.49$ m/s, in spite of the "Taylor" model assuming inviscid flow. It is smaller than the relative velocity for the large bubbles found in the air–water flows. This is thought to be due to the larger viscosity of the mud compared to the water.

The slope of the straight lines in the Zuber–Findlay plots, which is a function of the gas concentration and the liquid velocity profiles, was also independent of the mean void fraction. In the air–water flows at high void fractions, when the flow was dominated by large bubbles, the coefficient, C_0, was approximately unity. In this air–mud flow, however, it has been measured as $C_0 = 1.35$, indicating that the gas is being transported in a region in which the liquid flow rate is higher than the mean liquid flux rate. The slope of the Zuber–Findlay line is much greater in the mud flows than in the water flows and the relative velocity is only slightly less. We can therefore conclude that gas rise velocity in the viscous mud flow will be much greater than it would be in water for similar flow conditions.

7.3.2. Mud B

In order to investigate the mechanisms driving the flows seen with mud A, a second mud was tested which was intermediate in rheology between water and mud A. The rheograms are shown in figure 6.

The visual observations of the flow with this fluid showed some similarities with mud A, although it highlighted some very significant differences. As with mud A there was some evidence of small entrained bubbles being present in the flow. The volume fraction of these bubbles was much smaller than had been found with the other solution. It is thought that this is due to the yield stress of this fluid being much smaller than that of mud A.

The experimental results are shown in figure 17, where careful analysis shows that there is some variation in the relative velocity with void fraction, though much less than was seen with the air–water tests. Line fits are shown for the void fraction ranges 7.5–10 and 25–30%, which gave

$$v_G = 1.14 v_h = 0.39 \quad [30]$$

and

$$v_G = 1.14 v_h + 0.50, \quad [31]$$

respectively. The data for other void fractions showed transitional behaviour for the relative velocity between these two flow regimes, with similar values of C_0.

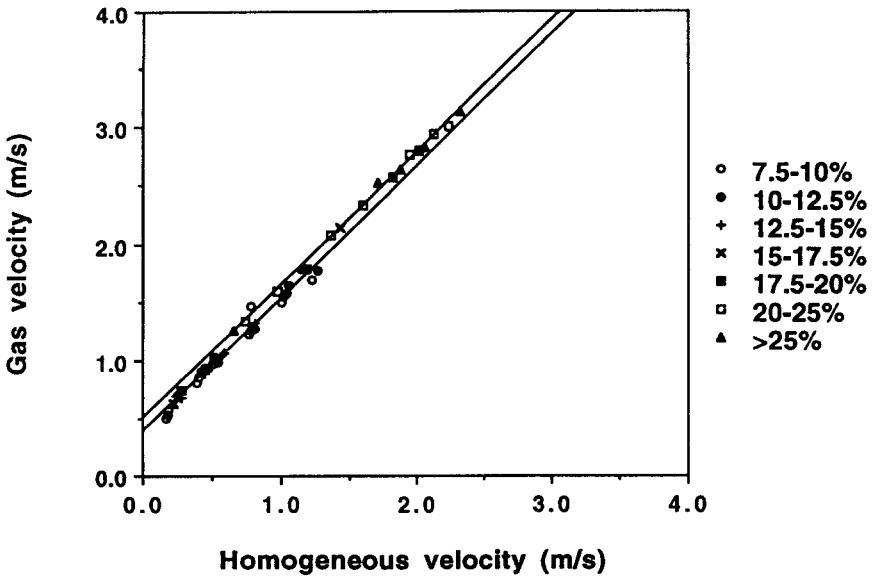

Figure 17. Zuber–Findlay plot for air–mud B flows in the pipe geometry.

These data show an intermediate behaviour between the water flows, where the relative velocity was heavily dependent upon the void fraction, and the mud A flows where it was independent of the void fraction. It is clear that the bubble size is weakly dependent upon the void fraction. The viscosity of the mud is sufficient to partially impede the bubble breakup process, but not as much as was seen with mud A.

The slope of the line in the Zuber–Findlay plot is also larger that that of water but less than that of the thicker mud. This means that the gas velocity is larger than it would be in water but smaller than if it were rising in the thicker mud.

8. CONCLUSION

It has been shown that in a larger pipe or annular geometry with air–water flows the behaviour can be characterized with the Zuber–Findlay (1965) model, [1], in which the coefficient C_0 is approx. 1.0 and the relative velocity, v_{rel}, varies with void fraction. The interpretation of C_0 has been confirmed by point measurements across the pipe. At low void fractions ($\bar{\epsilon} < 15\%$) the gas migration is by small bubbles. For high void fractions ($\bar{\epsilon} > 30\%$) the gas bubble relative velocity will be larger than a "Taylor"-type bubble rise speed. These results are in contrast to those for small pipe diameters, where the coefficient C_0 is approx. 1.2.

When air is injected into more viscous non-Newtonian, shear-thinning, fluids the gas migration is almost entirely by large bubbles. The size of these bubbles is independent of the mean void fraction but the frequency of these bubbles is variable. The transition to larger bubbles occurs at much lower void fractions than with water; for the more viscous fluid tested here the transition was complete at a very low void fraction ($\bar{\epsilon} < 7.5\%$). For fluids with an effective yield stress there will be small bubbles which will be held in suspension and will be transported with the liquid flow.

It was also shown that, whilst for the air–water flow the coefficient C_0 was approximately unity, for the more viscous fluids it is larger, indicating that the gas was being transported in a faster flowing region of the pipe and that the viscosity has modified the entire flow field.

The overall effect means that in more viscous fluids the gas migration velocity will be larger than would have been found for a similar condition in an air–water flow. The modification to the bubble distribution and flow field is more significant than any increased viscous drag on the bubble.

Acknowledgements—This work was carried out at Schlumberger Cambridge Research as part of a project on simulating gas kicks. It was partly funded by the U.K. Department of Energy. The author would like to thank the staff of the Fluid Mechanics Department at SCR for all their help in these experiments. In particular Roy (OGTB) Boardman and Paul Faupel, without whom nothing is possible, Dave Mackay and Steve Cooper,

who maintained most of the instrumentation, and Tim Holtan and Alan Mustafa, who ran many of the experiments. Also, Ian Walton made some very useful contributions on the dynamics of single bubbles and on the value of the experiments.

REFERENCES

AZIZ, K., GOVIER, G. W. & FOGARASI, M. 1972 Pressure drop in wells producing oil and gas. *J. Can. Pet.* **July,** 38–44.

BARNEA, D. & SHEMER, L. 1986 Rise velocity of large bubbles in stagnant liquid in non-circular ducts. *Int. J. Multiphase Flow* **12,** 1025–1027.

DAIRANIEH, I. S. & LAHALIH, S. M. 1988 Novel polymeric drilling mud viscosifiers. *Eur. Polym. J.* **24,** 831–835.

DAVIES, R. M. & TAYLOR, SIR G. I. 1950 The mechanics of large bubbles and rising through extended liquids and through liquids in tubes. *Proc. R. Soc.* **A200,** 375–390.

DUNS, H. & ROS, N. C. J. 1963 Vertical flow of gas and liquid mixtures in wells. Presented at the *6th World Petroleum Conf.*, Frankfurt.

GOVIER, G. W. & AZIZ, K. 1982 *The Flow of Complex Mixtures in Pipes.* Krieger, Malabar, FL.

HARMATHY, T. Z. 1960 Velocity of large drops and bubbles in media of infinite or restricted extent. *AIChE Jl* **6,** 281–288.

HERRINGE, R. A. & DAVIS, M. R. 1976 Structural development of gas–liquid flows. *J. Fluid Mech.* **73,** 97–123.

JOHNSON, A. B., HUNT, A. & WHITE, D. B. 1990 The effect of bubble coalescence on the development of multiphase flow. Presented at the *Int. Conf. on Heat and Mass Transfer: Phase Interface Phenomena in Multi-Phase*, Dubrovnik.

JONES O. C. JR & LEUNG, J. C. M. 1981 An improvement in the calculation of turbulent friction in a smooth concentric annuli. *ASME Jl Fluids Engng* **103,** 615–623.

KOWE, R., HUNT J. C. R., HUNT A., COUET, B. & BRADBURY, L. J. S. 1988 The effects of bubbles on the volume fluxes and the pressure gradients is non-uniform unsteady flow of liquids. *Int. J. Multiphase Flow* **14,** 587–606.

MASSEY, B. S. 1983 *Mechanics of Fluids.* Van Nostrand Rhinehold, Wokingham, Surrey, U.K.

METZNER, A. B. & PARK, M. G. 1964 Turbulent flow characteristics of viscoelastic fluids. *J. Fluid Mech.* **20,** 291–304.

NAKAGAWA, E. Y. & BOURGOYNE, A. T. 1989 Experimentally determined gas slip velocities in an inclined annulus. Presented at the *Int. Well Control Symp.*, LUS, Baton Rouge, LA.

PHILIP, J., PROCTOR, J. M., NIRANJAN, K. & DAVIDSON, J. F. 1990 Gas holdup and liquid circulation in internal loop reactors containing highly viscous Newtonian and non-Newtonian liquids. *Chem. Engng Sci.* **45,** 651–664.

RADER, D. W., BOURGOYNE, A. T. & WARD, R. H. 1975 Factors affecting bubble-rise velocity of gas kicks. *J. Pet. Technol.* **May,** 571–585.

SEKOGUCHI, K., FUKUI, H. & YOSHIFUSA, S. 1981 Flow characteristics and heat transfer in vertical bubble flow. In *Two Phase Flow Dynamics* (Edited by BERGLES, A. E. & ISHIGAT, S.), pp. 59–74. Hemisphere, London.

SKELLAND, A. H. P. 1967 *Non-Newtonian and Heat Transfer.* Wiley, New York.

VIGNEAUX, P., CHENAIS, P. & HULIN, J. P. 1988 Liquid–liquid flows in an inclinded pipe. *AIChE Jl* **34,** 781–789.

WALLIS, G. B. 1969 *One-dimensional Two-phase Flow.* McGraw Hill, New York.

VAN DER WELLE, R. 1985 Void fraction, bubble velocity and bubble size in two-phase flow. *Int. J. Multiphase Flow* **11,** 317–345.

WHALLEY, P. B. 1987 *Boiling, Condensation and Gas Liquid Flow.* Clarendon Press, Oxford.

ZUBER, N & FINDLAY, J. A. 1965 Average volumetric concentration in two-phase flow systems. *J. Heat Transfer* **88,** 453–468.

ZUBER, N. & HENCHE, J, 1962 Steady-state and transient void fraction of bubbling systems and their operating limits. Technical Report 62GL100, General Electric Co., Schenectady, NY.